ACS APPLIED NANO MATERIALS

www.acsanm.org
Article

Graphene Nanosheet-Gold Nanopatch Metasurfaces for Nonlinear Response at THz Frequencies

Anna Theodosi, Isaac Appiah Otoo, Anastasios D. Koulouklidis, Nikolaos Matthaiakakis, George Kakarantzas, Petri Mustonen, Harri Lipsanen, Georgy Fedorov, Ioannis Liontos, Stelios Tzortzakis, Polina Kuzhir, Maria Kafesaki, and Odysseas Tsilipakos*

Cite This: ACS Appl. Nano Mater. 2025, 8, 24473−24479
Read Online

ACCESS | Metrics & More | Article Recommendations | Supporting Information

ABSTRACT: Graphene's exceptional nonlinear optical properties combined with resonant photonic structures offer a promising pathway for efficient nonlinear applications at terahertz (THz) frequencies. In this work, we propose and demonstrate a fabrication-friendly hybrid nonlinear metasurface composed of gold patches integrated with uniform graphene, circumventing the need for complex graphene patterning. The structure supports strong localized resonances that enhance nonlinear interactions. By exploiting resonant enhancement at both the fundamental and third harmonic frequencies, we predict via simulations third-harmonic generation efficiencies as high as −15 dB (3.2%) under continuous-wave excitation at modest intensities (0.1 MW/cm^2). The metasurface is fabricated via electron-beam lithography and experimentally characterized under pulsed excitation using THz time-domain spectroscopy. The broadband excitation spectrum prevents unambiguous isolation of a third-harmonic signal; however, we experimentally observe pronounced nonlinear frequency shifts up to 0.5 THz (12.5% fractional change), driven by self-phase modulation, consistent with simulation results. Our findings highlight the potential of tailored graphene-based metasurfaces for efficient nonlinear THz photonic devices.

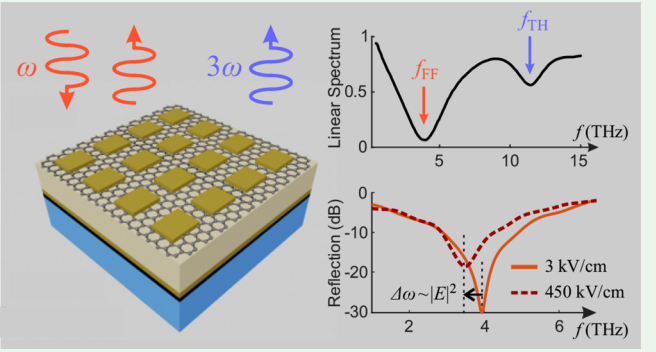

KEYWORDS: *third harmonic generation, nonlinear frequency shift, self-phase modulation, doubly resonant enhancement, metamaterials, nonlinear optics*

1. INTRODUCTION

Metasurfaces (MSs), ultrathin structures composed of a periodic arrangement of resonant meta-atoms on a plane, have attracted considerable research interest.[1,2] They have been shown to control the amplitude,[3] phase,[4] wavefront,[5] and polarization[6] of incident radiation targeting diverse applications such as wavefront manipulation,[5] spatial filtering[7], and (bio)sensing.[2,8] In order to enable nonlinear and reconfigurable MSs, materials with intensity-dependent and tunable properties should be exploited in the meta-atom geometry.[9−13] Nonlinearity, in particular, can significantly broaden the scope of achievable functionalities, enabling all-optical control and the generation of new frequencies. In this context, a unique 2D material for nonlinear MSs at THz frequencies is graphene,[14] which combines strong third order nonlinearity,[15−17] the ability to dynamically tune its linear and nonlinear properties via gating,[18,19] and the capability to support tightly confined surface plasmons.

The potential of graphene as a nonlinear material has been lucidly demonstrated in ref. 20, for instance, where high harmonic generation (up to seventh order) was obtained by a uniform graphene layer on a glass substrate. Patterning graphene into a metasurface can allow for fostering resonances, which enhance its interaction with light. By exploiting the corresponding energy confinement in space (small effective mode volume) and time (high quality factor), the efficiency of the nonlinear process can be further enhanced. This strategy has been leveraged for proposing efficient third harmonic generation[21−23] and all-optical polarization control,[24] among others. However, the patterning of graphene is an experimentally demanding procedure. To circumvent this difficulty, we propose here an experimentally friendlier and at the same time equally or even more efficient implementation, based on a uniform graphene layer, where the patterning is "transferred" to an adjacent gold layer. This approach still allows us to

Received: October 11, 2025
Revised: December 5, 2025
Accepted: December 8, 2025
Published: December 15, 2025

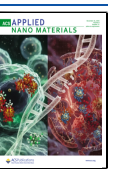

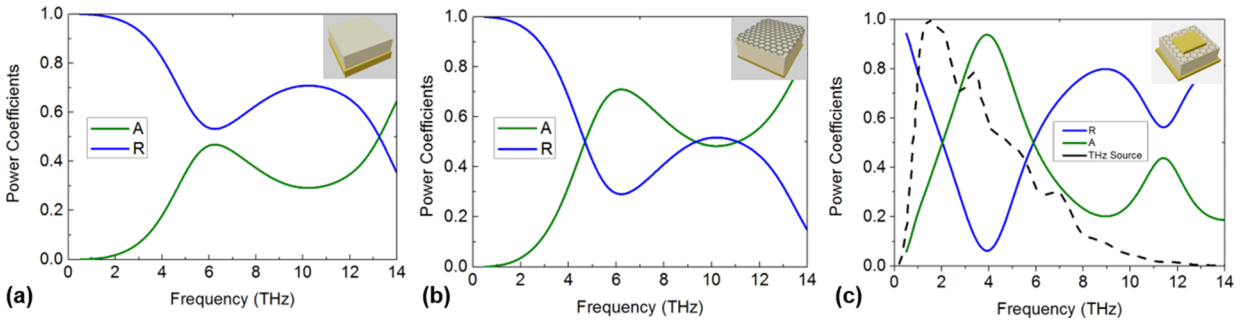

Figure 1. Design procedure of proposed hybrid gold-graphene metasurface. (a) By placing a gold back-reflector in an 8.3-μm-thick substrate, broad Fabry−Perot resonances are observed in the reflection (R) and absorption (A) power coefficients. (b) Uniform graphene layer on top of the gold-backed substrate leads to enhanced absorption. (c) Incorporating gold meta-atoms allows to excite graphene surface plasmons, and two well-defined resonances appear within the frequency range of interest. Proper selection of the gold patch dimensions allows to position the resonances at an $\omega - 3\omega$ configuration, which is desirable for doubly resonant enhancement of the third harmonic generation process. The dashed line in panel (c) shows the power spectrum of the THz source employed in the experimental characterization.

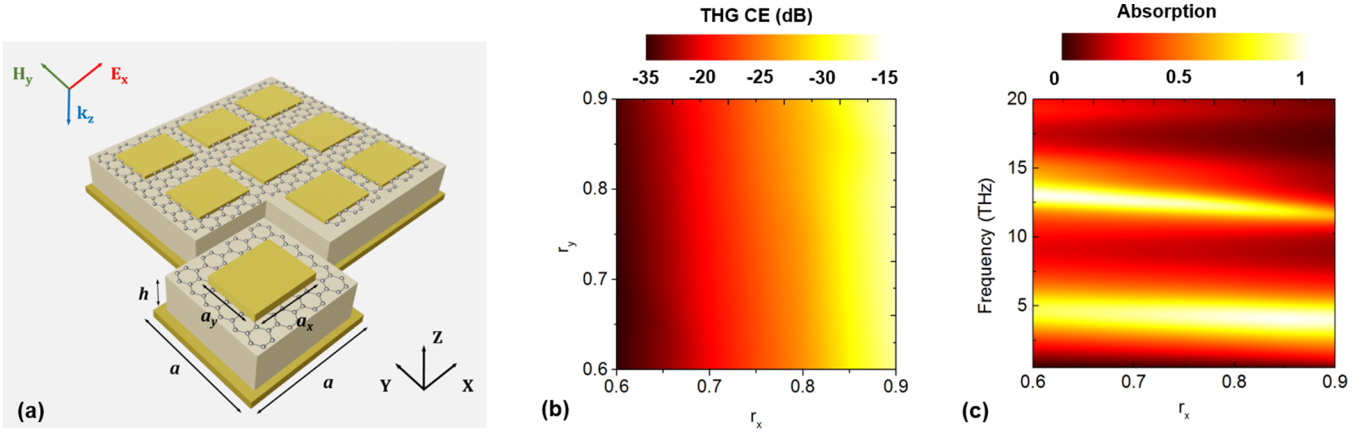

Figure 2. (a) Schematic of the proposed hybrid gold-graphene metasurface. The metasurface is composed of rectangular gold patches ($a_x \times a_y$) with thickness t = 500 nm and electric conductivity $\sigma = 4 \times 10^7$ S/m, placed in a square periodicity with period a = 5.6 μm. The patches reside on a graphene-covered polymer substrate (relative electric permittivity $\epsilon_r = 3.2 \times (1 - 0.1j)$ and thickness h = 8.3 μm), backed by a gold back reflector. The graphene layer is uniform, which helps with fabrication simplicity. The electric field of the incident wave is linearly polarized along the x-axis. (b) Calculated THG conversion efficiency (CE) under continuous plane wave illumination at normal incidence for an input intensity of I = 0.1 MW/cm^2, as a function of the gold patch size: $r_x = a_x/a$ and $r_y = a_y/a$. (c) Calculated linear absorption of the hybrid graphene metasurface, as a function of the frequency and patch size: $a_x = r_x \times a$ (r_y is constant at 0.65). The absorption peaks of the two resonances are placed at ∼4 and ∼12 THz for r_x = 0.9.

achieve strong resonances and tailor the resonant structure but without patterning graphene.

More specifically, we propose a hybrid gold-patch/uniform-graphene metasurface for enhancing nonlinear phenomena at THz frequencies. Note that a metal-stripes-on-uniform-graphene metasurface for frequency generation at THz frequencies has already been presented in the literature.[25] However, the 1D stripe geometry does not provide the necessary geometrical degrees of freedom to allow for tuning the underlying resonant structure. In this work, by varying the dimensions of the gold patches we can finely tune the resonant frequencies. It, thus, becomes possible to position two well-defined resonances at frequencies with ratio 1:3. Aligning resonances of the metasurface with the fundamental (FF) and third-harmonic (TH) frequencies is a well-known strategy for enhancing the conversion efficiency (CE) of the third harmonic generation (THG) process and is frequently termed doubly resonant enhancement.[22] Conversion efficiencies as high as −15 dB (3.2%) for an input intensity of 0.1 MW/cm^2 are theoretically predicted for continuous-wave operation, which are superior to previous approaches based on patterned graphene metasurfaces.[21,23] Subsequently, the proposed metasurface is fabricated via electron beam lithography and measured with a custom THz time-domain spectroscopy setup under pulsed excitation. As will be discussed in detail, due to the broad spectrum of the incident field extending up the regime of the third harmonic (and the absence of appropriate filtering components), it was not possible to experimentally discern a generated signal and assess the efficiency of the generation process. However, strong nonlinear frequency shifts up to 0.5 THz due to self-phase modulation are experimentally observed and verified by corresponding simulations. This pronounced nonlinear shift corresponds to a fractional decrease of the resonant frequency by 12.5% and can be used for nonlinearly switching between values of low and high reflection by tuning the input intensity.

2. RESULTS

2.1. Theoretical Analysis and Design. In Figure 1, the evolution of the design process for the hybrid gold-graphene metasurface is presented. Initially, by placing a gold back-reflector in an 8.3-μm-thick substrate, a broad Fabry−Perot

https://doi.org/10.1021/acsanm.5c04665
ACS Appl. Nano Mater. 2025, 8, 24473−24479

resonance is observed (Figure 1a). Incorporating a uniform graphene layer on top of the gold-backed substrate leads to enhanced absorption (Figure 1b), due to the real part of graphene's surface conductivity. However, in both cases a single resonance (absorption peak) appears in the frequency range of interest (0−14 THz). The integration of gold patches allows to excite surface plasmons on graphene (otherwise there is a momentum mismatch with free-space photons), leading to two well-defined resonances within the frequency window 0−14 THz (Figure 1c). By varying the shape and size of the gold meta-atoms, we can tune the resonant frequencies. For a specific combination of parameters, the two resonances are perfectly aligned at an $\omega - 3\omega$ configuration, which is the required condition to resonantly enhance both steps of the THG processes, namely, excitation at ω and radiation at 3ω. The desired positioning of the resonant frequencies is also related with the frequency content of our experimentally available THz source (for the corresponding spectrum see dashed line in panel Figure 1c). More specifically, the goal is to place the first resonance close to the peak of the pulse spectrum so as to best exploit the available field strength and allow the nonlinear processes to manifest. At the same time, we want to avoid exciting the second resonance with the input pulse, so that any recorded radiation at that frequency is solely attributed to the nonlinear harmonic generation process. We try to satisfy both constraints by placing the two frequencies at ∼4 and ∼12 THz, respectively.

Through this design evolution process we reach the metasurface geometry depicted in Figure 2a, where the main dimensions are also annotated. To arrive to this geometry we first make rational choices for the main unit cell dimensions: (i) the lattice constant is selected such that the array remains subwavelength even at the third harmonic frequency in order to avoid diffraction effects,[26] and (ii) the substrate thickness is tuned so that the fundamental resonance is placed near 4 THz, as discussed in the previous paragraph. The next step is to conduct a parametric study regarding the dimensions of the gold-meta-atoms to tune the alignment of the resonances at the $\omega - 3\omega$ configuration and to ensure the optimum performance. To enable extra degrees of freedom, we allow for a rectangular patch geometry, meaning that the metasurface response will differ for the two orthogonal linear polarizations. Unless otherwise noted, the incident wave is a normally incident linearly polarized (E_x) plane wave, as depicted in the inset of Figure 2a. This optimization process is based on maximizing the calculated third harmonic generation. The simulations are conducted using the commercial software COMSOL Multiphysics under continuous wave conditions by utilizing two independent frequency-domain linear simulations. Details can be found in the Supporting Information (Section S1, Figure S1). The gold meta-atoms with size $a_x \times a_y$, thickness t = 500 nm and electric conductivity $\sigma = 4 \times 10^7$ S/m, are placed in a square periodicity with period a = 5.6 μm, on top of a polymeric (parylene) substrate with relative electric permittivity $\epsilon_r = 3.2 \times (1 - 0.1j)$ and thickness h = 8.3 μm. The adopted permittivity is an average value of the measured data at low THz frequencies,[27] since dispersion is weak. A unit cell of the metasurface (periodic boundary conditions at the xz and yz planes) is used in the simulations. Graphene is modeled using appropriate dispersive linear and third-order nonlinear conductivities[21,28] via the surface current boundary condition. The gold backreflector is significantly thicker than the skin depth at low THz frequencies; thus, transmission is hindered and the metasurface operates in reflection.

For the parametric study, we vary r_x and r_y ($r_x = a_x/a$ and $r_y = a_y/a$) in the range 0.6−0.9 and calculate the corresponding THG efficiency (Figure 2b). The input intensity is set to I = 0.1 MW/cm^2 and the THG conversion efficiency (CE) was defined as the ratio of power radiated at the third harmonic to the input power at the fundamental frequency (P_{TH}/P_{FF}). In each case, the third harmonic frequency was chosen to match the second (and narrower) absorption peak of the metasurface (see Figure 1c), while the operating (or fundamental) frequency is one-third of this value. The maximum CE was calculated to be −15 dB (∼ 3.2%) for the combination r_x = 0.9 and r_y = 0.65. To verify that the physical origin of this high efficiency is the doubly resonant enhancement, in Figure 2c we plot the linear absorption of the hybrid graphene metasurface as a function of the frequency and patch size: $a_x = r_x \times a$. The size of the patch along the y-axis is held constant at r_y = 0.65. Results for other values of the parameter r_y are presented the Supporting Information (Section S2, Figure S2). As shown in Figure 2c, the two resonances are placed at frequencies ∼4 and ∼12 THz that best satisfy the $\omega - 3\omega$ relation for the value r_x = 0.9.

We can further study the electromagnetic response of the optimum metasurface (r_x = 0.9 and r_y = 0.65) by correlating eigenmode analysis and scattering simulations. In Figure 3a, we plot the power coefficients for linear plane-wave scattering

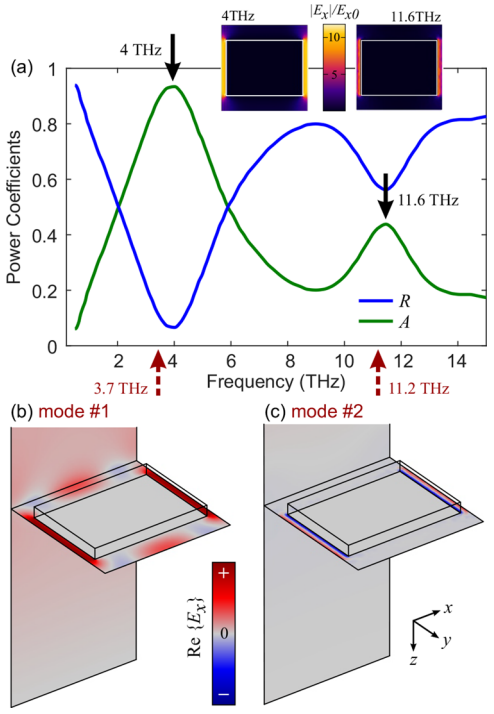

Figure 3. Analysis of the optimum gold-graphene metasurface with r_x = 0.90 and r_y = 0.65. (a) Reflection ($R = |r|^2$) and Absorption (A) power coefficients of the metasurface obtained from linear plane-wave scattering simulations. The positions of the absorption peaks are marked with black solid arrows. The field enhancement $|E_x|/|E_{x0}|$ at these frequencies, calculated at the plane of graphene, is depicted in the insets. The corresponding eigenfrequencies obtained from eigenmode analysis are marked with red dashed arrows. (b, c) Mode profile (E_x component, real part) of the two eigenmodes, shown in a perspective view of the metasurface unit cell.

https://doi.org/10.1021/acsanm.5c04665
ACS Appl. Nano Mater. 2025, 8, 24473−24479

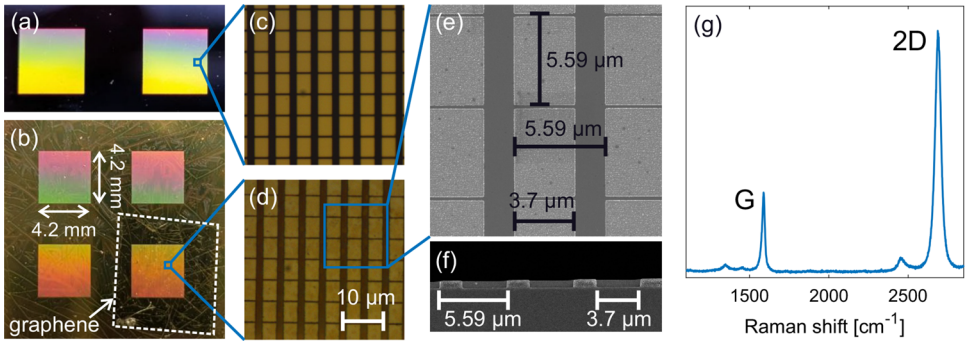

Figure 4. (a, c) Photograph and optical microscopy image of a test metasurface comprising gold patches on a silicon substrate. (b, d) Photograph and optical microscopy image of proposed metasurfaces (4.2 mm × 4.2 mm lateral size each) with configuration: silicon wafer, gold backreflector, parylene, gold patches. Graphene has been introduced in the lower right area (shown with a dashed white square). The overall structural quality remains consistent between the test structure and the proposed metasurface. (e) Top-view and (f) cross-sectional SEM images of the graphene-based metasurface after development. (g) Raman spectrum of a single layer of graphene transferred onto the metasurface. The two characteristic graphene G (1589 cm^{-1}) and 2D (2689 cm^{-1}) peaks are evident.

(reflection: blue; absorption: green). With black arrows we mark the positions of the two absorption peaks at 4 THz and 11.6 THz, respectively. At these frequencies, the local field enhancement is maximized leading to increased absorption as well. By plotting the ratio $|E_x|/|E_{x0}|$ on the plane of graphene (inset in Figure 3a), we find that the enhancement reaches a value of ∼10 for the first peak and ∼7 for the second one. Finally, we use eigenmode analysis to calculate the eigenmodes of the metasurface. We verify that the two absorption peaks are directly associated with two eigenfrequencies of the metasurface at 3.7 THz and 11.2 THz, respectively (see red arrows in Figure 3a). This is confirmed by comparing the field distribution in the scattering simulations at the absorption peaks with the two said eigenvectors. The two eigenmodes (E_x component, real part) are plotted in Figure 3b,c, respectively. The distinct nature of the two modes can be clearly discerned.

We should note that the rectangular shape of the gold patches ($r_y \neq r_x$) leads to different response for the E_x or E_y linear polarizations. For isotropic response, a unit cell with C_{4v} rotational symmetry is required.[29] As illustrated in one of our earlier works,[23] this could be addressed by using a cross geometry comprised of two rectangles perpendicular with each other.

2.2. Experimental Demonstration. We proceed with the experimental demonstration. We first describe step-by-step the fabrication process. Next, we present the material and structural characterization via Raman spectroscopy of the graphene monolayer and scanning electron microscope (SEM) images of the fabricated metasurface. Finally, we present the THz time-domain spectroscopy setup employed for the electromagnetic characterization and the corresponding measurements.

The metasurface samples were fabricated using 100-mm diameter, single-sided polished silicon wafers (525 ± 25-μm thick, doped with phosphorus and boron, resistivity 1−30 Ωcm). The wafers were cleaved into 2.5 cm × 2.5 cm pieces (about 0.98 square inches), cleaned sequentially in acetone and isopropanol using ultrasonic baths (5 min each), and dried with nitrogen gas. A 5 nm titanium adhesion layer was deposited, followed by 200 nm of gold via thermal evaporation. A parylene layer (8.3-μm thick) was then deposited, and a monolayer of graphene was transferred on top. To define the metasurface, an electron beam resist (AR-P 671.11) was spin-coated and baked (150 °C, 5 min), followed by electron beam lithography exposure and development. A 5 nm chromium adhesion layer and 200 nm of gold were then deposited to form the patches. After lift-off in acetone (12 h) and rinsing in isopropanol, the samples were dried with nitrogen. A schematic of the fabrication process flow along with extra details can be found in the Supporting Information, Section S3 (Figure S3).

A photograph and optical microscopy image of the fabricated hybrid gold-graphene metasurface are shown in Figure 4b,d, respectively. Each metasurface measures approximately ∼4.2 mm × 4.2 mm across and comprises roughly 700 × 700 unit cells, corresponding to ∼165 free space wavelengths at the third harmonic frequency (12 THz). Graphene has been introduced in the lower right area (shown with a dashed white line). Compared with a test structure of gold patches on a silicon substrate (Figure 4a,c), the overall structural quality remains consistent. SEM inspection confirms the accurate fabrication of the gold meta-atoms (Figure 4e,f). The exact measured lattice constant is 5.59 μm, almost perfectly matching the design value of 5.6 μm. Structures with r_x up to 0.95 and well-defined 280 nm gaps were fabricated. Raman spectroscopy verified the presence of monolayer graphene, revealing characteristic G (1589 cm^{-1}) and 2D (2689 cm^{-1}) peaks (Figure 4g).

The fabricated graphene-gold samples were electromagnetically characterized using a custom THz time-domain spectroscopy (THz-TDS) setup. Broadband THz pulses with peak electric fields up to 450 kV/cm were generated via two-color filamentation of ultrashort laser pulses in air.[30] The resulting THz electric field employed in the experiments, along with the corresponding spectrum, can be found in the Supporting Information (Section S4, Figure S4b). In order to control the THz field strength, the THz beam after being generated with the highest strength was directed through a pair of wire-grid polarizers to enable intensity control and achieve different field strengths while preserving the polarization state of the THz pulse. Then the beam illuminated the sample under TM polarization at an incidence angle of 16°. The reflected THz radiation was detected using air-biased coherent detection (ABCD), which provides access to the full spectral content of the THz pulse without interference from phonon resonances. For each field strength, the recorded reflection spectra are normalized to a corresponding reference case without the sample (a bare gold reflector) and recorded under identical conditions. We also note that the wire-grid polarizers used to

https://doi.org/10.1021/acsanm.5c04665
ACS Appl. Nano Mater. 2025, 8, 24473−24479

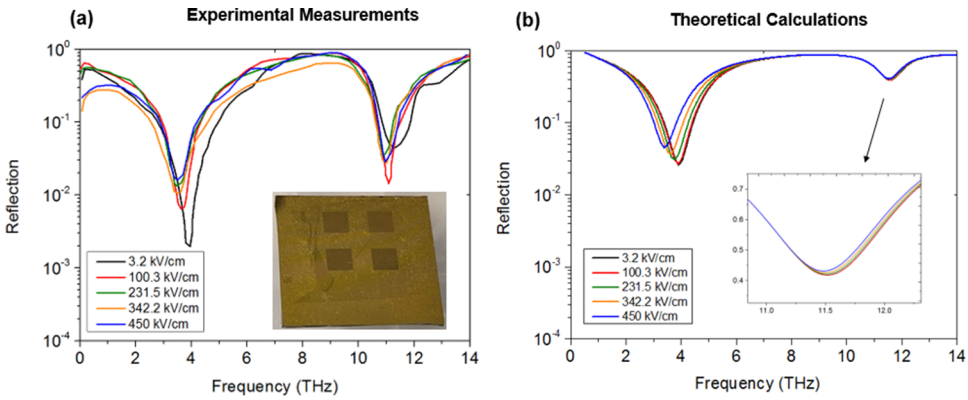

Figure 5. (a) Experimental THz-TDS reflection spectra of the fabricated hybrid gold-graphene metasurface (shown in the inset) for different values of incident electric field strength. (b) Corresponding calculations (zoom in for the second resonance in the inset).

control the field strength feature a relatively flat spectral transmission over the range of interest. This procedure eliminates any potential spectral variations or intensity-dependent distortions in the incident THz pulse. A schematic of the employed THz-TDS setup can be can be found in the Supporting Information (Section S4, Figure S4a).

The experimentally measured reflection spectra are presented in Figure 5a as a function of the electric field amplitude $|E_0|$, varying from 3.2 kV/cm up to 450 kV/cm. The two reflection dips near 4 and 12 THz are clearly visible. Evidently, increasing the input intensity leads to a redshift of both resonances. This nonlinear self-shift is due to self-phase modulation.[31] The effect is more pronounced for the first resonance due to the stronger overlap of the mode profile with graphene. In fact, this shift reaches ~0.5 THz (corresponds to a fractional decrease of 12.5% for the resonant frequency) and can be used for nonlinearly switching between values of low and high reflection by tuning the input intensity. The contrast (or extinction ratio, ER) can exceed 16 dB when the operating frequency coincides with the first minimum of the black curve in Figure 5a. The magnitude of the nonlinear shift measured experimentally can be also verified by numerical simulations. The calculations are presented in Figure 5b and are in good agreement with the experimental measurements. To illustrate the change in material properties that is required to induce the 0.5 THz frequency shift, we focus in the neighborhood of 4THz, where the first resonance lies, and adopt a dispersionless surface conductivity of 348 + 395j μS by using eq (S1). Since $\sigma^{(3)}$ given by eq (S3) is purely imaginary, we next vary the imaginary part of the adopted $\sigma^{(1)}$ value (which physically is the one that is anticipated to affect the resonance frequency). We find that the 0.5 THz shift can be reproduced by a conductivity change in the order of 40%, see Figure S5 in the Supporting Information.

However, we were not able to identify a definitive feature indicating third harmonic generation. This arises because the TH field is generated simultaneously with the reflected pump pulse, leading to complete temporal overlap. Moreover, the broadband pump retains appreciable spectral content even in the frequency range where the third harmonic is expected (cf. Figure 1c); the much weaker TH generated signal is masked by this background and does not emerge as a distinct spectral feature. We have verified this assumption by resorting to time-domain nonlinear simulations. The simulations were conducted using the commercial software Ansys Lumerical FDTD implementing the Finite-Difference Time-Domain method. In these simulations we have used three incident source signals with different bandwidths and the results are included in the Supporting Information (Section S6, Figure S6). Briefly, when using a broadband input imitating the actual THz source, a distinct peak of THG cannot be observed in the reflection power spectra. On the other extreme, when we use a narrow source with a bandwidth of 300 GHz, we can identify a clear strong peak of THG. Finally, to verify beyond doubt that the observed peak in the time-domain simulations corresponds to THG, we have performed a sweep of the input power and extracted the generated power at the third harmonic frequency. As shown in the Supporting Information (Figure S7), the system follows the power scaling law of the third-order process. We therefore concluded that in order to verify the capabilities of the proposed metasurface for efficient THG, the bandwidth of the input pulse should be reduced. However, attempts to directly affect the source bandwidth in the experiment led to significantly limiting the source intensity and, consequently, the efficiency of the nonlinear process. To overcome this limitation, future optimization of the detection scheme will employ multiple bandpass THz filters to suppress the broadband pump contribution prior to incidence on the sample, thereby eliminating its overlap in the spectral region around the expected TH and enabling clearer isolation of the TH signal.

Thus, far, theoretical calculations have been performed under normal incidence. However, in the experimental setup we are forced to deviate from the normal by a small incidence angle (16°). Thus, we next studied the effect of the incidence angle on the response of the metasurface, for both TM and TE polarizations. In the Supporting Information (Section S7, Figures S8 and S9) we include both linear reflection/absorption spectra and the calculated third harmonic generation efficiency. It can be seen that oblique incidence affects the resonance frequencies and the corresponding absorption peak (reflection dip). As a result, it can affect the THG efficiency, when it deviates considerably from normal incidence for which the metasurface dimensions have been designed. The effect is more detrimental for the TM polarization.

Before concluding, we should note that we have modeled the third-order nonlinearity of graphene with a simple dispersive $\sigma^{(3)}$ conductivity.[28] More accurate descriptions (hot electron models[32]) are important for assessing graphene's nonlinear response in pulsed conditions. However, we note that the design procedure (Section 2.1 and Figure 2) is

https://doi.org/10.1021/acsanm.5c04665
ACS Appl. Nano Mater. 2025, 8, 24473−24479

conducted in CW conditions and it assesses different designs in a comparative manner. That is, the optimum design should still be valid irrespective of the actual model for graphene's nonlinearity.

3. CONCLUSIONS

In conclusion, we have proposed a hybrid gold-patch/uniform-graphene nonlinear metasurface that offers a fabrication-friendly alternative to patterned graphene architectures, while at the same time delivering highly nonlinear response. Our theoretical analysis predicts third-harmonic generation efficiencies reaching −15 dB (3.2%) under continuous-wave excitation at modest input intensities of 0.1 MW/cm^2. The metasurface was fabricated via electron-beam lithography and characterized using terahertz time-domain spectroscopy under pulsed excitation. Notably, we experimentally observed pronounced nonlinear spectral shifts of up to 0.5 THz attributed to self-phase modulation, in excellent agreement with simulation results. While third-harmonic generation was not experimentally resolved due to the broadband nature of the excitation pulse, our simulations indicate that the metasurface is capable of efficient THG under narrowband excitation. Altogether, these findings underscore the promise of resonance-engineered graphene-based metasurfaces as a versatile platform for advanced nonlinear photonic functionalities.

■ ASSOCIATED CONTENT

Supporting Information

The Supporting Information is available free of charge at https://pubs.acs.org/doi/10.1021/acsanm.5c04665.

Extra modeling details, additional results (nonlinear response for variable source bandwidth, response under oblique incidence, etc.), detailed description of the fabrication process and the THz-TDS measurement setup (PDF)

■ AUTHOR INFORMATION

Corresponding Author

Odysseas Tsilipakos − *Theoretical and Physical Chemistry Institute, National Hellenic Research Foundation, 11635 Athens, Greece;* orcid.org/0000-0003-4770-0955; Email: otsilipakos@eie.gr

Authors

Anna Theodosi − *Institute of Electronic Structure and Laser, Foundation for Research and Technology Hellas, 70013 Heraklion, Greece; Department of Materials Science and Engineering, University of Crete, 70013 Heraklion, Greece*

Isaac Appiah Otoo − *Department of Physics and Mathematics, University of Eastern Finland, 80101 Joensuu, Finland;* orcid.org/0000-0002-8999-8684

Anastasios D. Koulouklidis − *Institute of Electronic Structure and Laser, Foundation for Research and Technology Hellas, 70013 Heraklion, Greece; Regensburg Center for Ultrafast Nanoscopy (RUN) and Department of Physics, University of Regensburg, 93040 Regensburg, Germany;* orcid.org/0000-0003-4191-0089

Nikolaos Matthaiakakis − *Institute of Nanoscience and Nanotechnology, National Center for Scientific Research "Demokritos", 15341 Athens, Greece*

George Kakarantzas − *Theoretical and Physical Chemistry Institute, National Hellenic Research Foundation, 11635 Athens, Greece*

Petri Mustonen − *Department of Electronics and Nanoengineering, Aalto University, 02150 Espoo, Finland*

Harri Lipsanen − *Department of Electronics and Nanoengineering, Aalto University, 02150 Espoo, Finland;* orcid.org/0000-0003-2487-4645

Georgy Fedorov − *Department of Physics and Mathematics, University of Eastern Finland, 80101 Joensuu, Finland*

Ioannis Liontos − *Institute of Electronic Structure and Laser, Foundation for Research and Technology Hellas, 70013 Heraklion, Greece*

Stelios Tzortzakis − *Institute of Electronic Structure and Laser, Foundation for Research and Technology Hellas, 70013 Heraklion, Greece; Department of Materials Science and Engineering, University of Crete, 70013 Heraklion, Greece*

Polina Kuzhir − *Department of Physics and Mathematics, University of Eastern Finland, 80101 Joensuu, Finland;* orcid.org/0000-0003-3689-0837

Maria Kafesaki − *Institute of Electronic Structure and Laser, Foundation for Research and Technology Hellas, 70013 Heraklion, Greece; Department of Materials Science and Engineering, University of Crete, 70013 Heraklion, Greece;* orcid.org/0000-0002-9524-2576

Complete contact information is available at: https://pubs.acs.org/10.1021/acsanm.5c04665

Funding

The open access publishing of this article is financially supported by HEAL-Link.

Notes

The authors declare no competing financial interest.

■ ACKNOWLEDGMENTS

The authors acknowledge the EU Horizon 2020 MSCA project 01007896 (CHARTIST), the Research Council of Finland (Flagship Programme PREIN, decisions no. 368653 and 368652 and research project decisions no. 343393 and 358812), and the Hellenic Foundation for Research and Innovation (H.F.R.I.) under the "2nd Call for H.F.R.I. Research Projects to support Post-doctoral Researchers"(Project No. 916, PHOTOSURF) and under the "2nd Call for H.F.R.I. Research Projects to support Faculty members and Researchers"(Project Number: 4542).

■ REFERENCES

(1) Quevedo-Teruel, O.; et al. Roadmap on metasurfaces. *Journal of Optics* **2019**, *21*, No. 073002.

(2) Wang, Y.; Zhang, X.; Wang, Y.; Liu, Y.; Li, J.; Chen, X.; Cui, Z.; Burokur, S. N.; Zhang, J.; Zhao, X.; Zhang, K.; You, Z. Recent Advances in Metasurfaces: From THz Biosensing to Microwave Wireless Communications. *Research* **2025**, *8*, No. 0820.

(3) Liu, X.; Fan, K.; Shadrivov, I. V.; Padilla, W. J. Experimental realization of a terahertz all-dielectric metasurface absorber. *Opt. Express* **2017**, *25*, 191−201.

(4) Tsilipakos, O.; Koschny, T. Multiresonant metasurfaces for arbitrarily broad bandwidth pulse chirping and dispersion compensation. *Phys. Rev. B* **2023**, *107*, No. 165408.

(5) Tsilipakos, O.; Kafesaki, M.; Economou, E. N.; Soukoulis, C. M.; Koschny, T. Squeezing a Prism into a Surface: Emulating Bulk Optics

with Achromatic Metasurfaces. *Adv. Opt. Mater.* **2020**, *8*, No. 2000942.
(6) Orazbay, M.; Valagiannopoulos, C. Twistronics-based polarization engineering. *Physical Review Applied* **2024**, *22*, No. 054028.
(7) Liu, T.; Qiu, J.; Xu, L.; Qin, M.; Wan, L.; Yu, T.; Liu, Q.; Huang, L.; Xiao, S. Edge Detection Imaging by Quasi-Bound States in the Continuum. *Nano Lett.* **2024**, *24*, 14466−14474.
(8) Xomalis, A.; Tsilipakos, O.; Manousidaki, M.; De Gregorio, P.; Busquets, O.; Kenanakis, G.; Tzortzakis, S.; Farsari, M.; Soukoulis, C. M.; Economou, E. N.; Kafesaki, M. Enhanced Refractive Index Sensing with Direction-Selective Three-Dimensional Infrared Metamaterials. *ACS Appl. Opt. Mater.* **2023**, *1*, 10−16.
(9) Gorecki, J.; Piper, L.; Noual, A.; Mailis, S.; Papasimakis, N.; Apostolopoulos, V. Optically Reconfigurable Graphene/Metal Metasurface on Fe:LiNbO3 for Adaptive THz Optics. *ACS Applied Nano Materials* **2020**, *3*, 9494−9501.
(10) Tao, Y.; Fang, B.; Pan, G.-M.; Zhang, D.-Q.; Jin, Z.-W.; Hong, Z.; Shu, F.-Z. Tunable High-Q Resonance Based on Hybrid Phase-Change Metasurfaces. *ACS Applied Optical Materials* **2023**, *1*, 1452−1459.
(11) Savarese, P.; Bansal, S.; Ammendola, M. G.; Barboza, R.; Salvatore, M.; Oscurato, S. L.; Piccirillo, B.; Di Colandrea, F.; Marrucci, L.; Cardano, F. Electrically tunable liquid-crystal metasurfaces with patterned birefringence and dichroism. *APL Photonics* **2025**, *10*, No. 050802.
(12) Gu, L.; Zhou, Y. Nonlinear optics in 2D materials: From classical to quantum. *Appl. Phys. Rev.* **2025**, *12*, No. 011335.
(13) Sun, G.; Wang, Y.; Cui, Z.; Xie, R.; Zhao, X. Enhanced terahertz high-harmonic generation from high-Q quasi-bound states in the continuum empowered by permittivity-broken metasurface. *Appl. Phys. Lett.* **2024**, *124*, 111704.
(14) Vermeulen, N. Perspectives on nonlinear optics of graphene: Opportunities and challenges. *APL Photonics* **2022**, *7*, No. 020901.
(15) Mikhailov, S. A. Theory of the strongly nonlinear electrodynamic response of graphene: A hot electron model. *Phys. Rev. B* **2019**, *100*, No. 115416.
(16) Dremetsika, E.; Dlubak, B.; Gorza, S.-P.; Ciret, C.; Martin, M.-B.; Hofmann, S.; Seneor, P.; Dolfi, D.; Massar, S.; Emplit, P.; Kockaert, P. Measuring the nonlinear refractive index of graphene using the optical Kerr effect method. *Opt. Lett.* **2016**, *41*, 3281.
(17) Koulouklidis, A. D.; Tasolamprou, A. C.; Doukas, S.; Kyriakou, E.; Ergoktas, M. S.; Daskalaki, C.; Economou, E. N.; Kocabas, C.; Lidorikis, E.; Kafesaki, M.; Tzortzakis, S. Ultrafast Terahertz Self-Induced Absorption and Phase Modulation on a Graphene-Based Thin Film Absorber. *ACS Photonics* **2022**, *9*, 3075−3082.
(18) Alexander, K.; Savostianova, N. A.; Mikhailov, S. A.; Van Thourhout, D.; Kuyken, B. Gate-Tunable Nonlinear Refraction and Absorption in Graphene-Covered Silicon Nitride Waveguides. *ACS Photonics* **2018**, *5*, 4944−4950.
(19) Amanatiadis, S.; Karamanos, T.; Lemoult, F.; Kantartzis, N. V. Enhanced mm-Wave Frequency Up-Conversion via a Time-Varying Graphene Aperture on a Cavity Resonator. *Micromachines* **2025**, *16*, 679.
(20) Hafez, H. A.; et al. Extremely efficient terahertz high-harmonic generation in graphene by hot Dirac fermions. *Nature* **2018**, *561*, 507−511.
(21) Jin, B.; Guo, T.; Argyropoulos, C. Enhanced third harmonic generation with graphene metasurfaces. *Journal of Optics* **2017**, *19*, No. 094005.
(22) You, J. W.; You, J.; Weismann, M.; Panoiu, N. C. Double-resonant enhancement of third-harmonic generation in graphene nanostructures. *Philosophical Transactions of the Royal Society A: Mathematical, Physical and Engineering Sciences* **2017**, *375*, 20160313.
(23) Theodosi, A.; Tsilipakos, O.; Soukoulis, C. M.; Economou, E. N.; Kafesaki, M. 2D-patterned graphene metasurfaces for efficient third harmonic generation at THz frequencies. *Opt. Express* **2022**, *30*, 460−472.
(24) Matthaiakakis, N.; Droulias, S.; Kakarantzas, G. Ultrafast All-Optical Control of Multiple Light Degrees of Freedom through Mode Mixing in a Graphene Nanoribbon Metamaterial for Modulation of Electromagnetic Waves. *ACS Applied Nano Materials* **2025**, *8*, 16499−16508.
(25) Deinert, J.-C.; et al. Grating-Graphene Metamaterial as a Platform for Terahertz Nonlinear Photonics. *ACS Nano* **2021**, *15*, 1145−1154.
(26) Christopoulos, T.; Nousios, G.; Kriezis, E. E.; Tsilipakos, O. Quasinormal mode theory for multiresonant metasurfaces with superwavelength periodicity involving two-dimensional materials. *Phys. Rev. B* **2024**, *110*, No. 245407.
(27) Liu, X.; MacNaughton, S.; Shrekenhamer, D. B.; Tao, H.; Selvarasah, S.; Totachawattana, A.; Averitt, R. D.; Dokmeci, M. R.; Sonkusale, S.; Padilla, W. J. Metamaterials on parylene thin film substrates: Design, fabrication, and characterization at terahertz frequency. *Appl. Phys. Lett.* **2010**, *96*, No. 011906.
(28) Cheng, J. L.; Vermeulen, N.; Sipe, J. E. Third order optical nonlinearity of graphene. *New J. Phys.* **2014**, *16*, No. 053014.
(29) Liu, T.; Qin, M.; Qiu, J.; Tu, X.; Qiu, H.; Wu, F.; Yu, T.; Liu, Q.; Xiao, S. Polarization-Independent Enhancement of Third-Harmonic Generation Empowered by Doubly Degenerate Quasi-Bound States in the Continuum. *Nano Lett.* **2025**, *25*, 3646−3652.
(30) Koulouklidis, A. D.; Gollner, C.; Shumakova, V.; Fedorov, V. Y.; Pugžlys, A.; Baltuška, A.; Tzortzakis, S. Observation of extremely efficient terahertz generation from mid-infrared two-color laser filaments. *Nat. Commun.* **2020**, *11*, 292.
(31) Christopoulos, T.; Tsilipakos, O.; Kriezis, E. E. Temporal coupled-mode theory in nonlinear resonant photonics: From basic principles to contemporary systems with 2D materials, dispersion, loss, and gain. *J. Appl. Phys.* **2024**, *136*, No. 011101.
(32) Massicotte, M.; Soavi, G.; Principi, A.; Tielrooij, K.-J. Hot carriers in graphene − fundamentals and applications. *Nanoscale* **2021**, *13*, 8376−8411.

https://doi.org/10.1021/acsanm.5c04665
ACS Appl. Nano Mater. 2025, 8, 24473−24479